

Mechanistic understanding of catechols and integration into an electrochemically cross-linked mussel foot inspired adhesive hydrogel

Cite as: Biointerphases 16, 061002 (2021); <https://doi.org/10.1116/6.0001609>

Submitted: 09 November 2021 • Accepted: 06 December 2021 • Published Online: 30 December 2021

 Julia Appenroth, Laila Moreno Ostertag,  Alexander M. Imre, et al.



View Online



Export Citation



CrossMark

ARTICLES YOU MAY BE INTERESTED IN

[Novel in situ sensing surface forces apparatus for measuring gold versus gold, hydrophobic, and biophysical interactions](#)

Journal of Vacuum Science & Technology A **39**, 023201 (2021); <https://doi.org/10.1116/6.0000611>

[Recent advances of luminogens with aggregation-induced emission in multi-photon theranostics](#)

Applied Physics Reviews **8**, 041328 (2021); <https://doi.org/10.1063/5.0071142>

[A computational framework for patient-specific surgical planning of type 1 thyroplasty](#)
JASA Express Letters **1**, 125203 (2021); <https://doi.org/10.1121/10.0009084>



Advance your science and
career as a member of

AVS

LEARN MORE



Mechanistic understanding of catechols and integration into an electrochemically cross-linked mussel foot inspired adhesive hydrogel

Cite as: *Biointerphases* 16, 061002 (2021); doi: 10.1116/6.0001609

Submitted: 9 November 2021 · Accepted: 6 December 2021 ·

Published Online: 30 December 2021



View Online



Export Citation



CrossMark

Julia Appenroth,^{1,2}  Laila Moreno Ostertag,¹ Alexander M. Imre,¹  Markus Valtiner,^{1,a)}  and Laura L. E. Mears^{1,a)} 

AFFILIATIONS

¹Institute of Applied Physics, Vienna University of Technology, 1040 Vienna, Austria

²CEST Centre for Electrochemistry and Surface Technology GmbH, Viktor-Kaplan-Strasse 2 Bauteil A, 2700 Wr. Neustadt, Austria

^{a)}Authors to whom correspondence should be addressed: valtiner@iap.tuwien.ac.at and mears@iap.tuwien.ac.at

ABSTRACT

Catechol reaction mechanisms form the basis of marine mussel adhesion, allowing for bond formation and cross-linking in wet saline environments. To mimic mussel foot adhesion and develop new bioadhesive underwater glues, it is essential to understand and learn to control their redox activity as well as their chemical reactivity. Here, we study the electrochemical characteristics of functionalized catechols to further understand their reaction mechanisms and find a stable and controllable molecule that we subsequently integrate into a polymer to form a highly adhesive hydrogel. Contradictory to previous hypotheses, 3,4-dihydroxy-L-phenylalanine is shown to follow a Schiff-base reaction whereas dopamine shows an intramolecular ring formation. Dihydrocaffeic acid proved to be stable and was substituted onto a poly(allylamine) backbone and electrochemically cross-linked to form an adhesive hydrogel that was tested using a surface forces apparatus. The hydrogel's compression and dehydration dependent adhesive strength have proven to be higher than in mussel foot proteins (mfp-3 and mfp-5). Controlling catechol reaction mechanisms and integrating them into stable electrochemically depositable macroscopic structures is an important step in designing new biological coatings and underwater and biomedical adhesives.

© 2021 Author(s). All article content, except where otherwise noted, is licensed under a Creative Commons Attribution (CC BY) license (<http://creativecommons.org/licenses/by/4.0/>). <https://doi.org/10.1116/6.0001609>

I. INTRODUCTION

Catechols are a central chemical motif in a variety of biochemical processes. These include electrochemical signaling, adhesion promotion, and redox mediation in both the respiratory and photosynthetic cycles. Essentially, they are found in all living organisms and a wide variety of natural environments. Certain marine organisms, such as mussels, have developed sophisticated adhesive proteins with a high (up to 30%) content of the redox-active 3,4-dihydroxy-L-phenylalanine (L-DOPA) amino acid in the sequence to increase their adhesive power to organic and inorganic surfaces in wet and high salinity environments.^{1–3} The oxidation/reduction behavior of catechols has been found to support a precisely controlled reactive environment, mediating interfacial adhesion and cross-linking, and, hence, cohesion in mussel foot structures.⁴

In particular, the controlled local presence of L-DOPA in a mussel foot appears to add to these properties, as it is represented in the mussel foot proteins (mfp).^{1,3,5} The L-DOPA content varies between the different mfp,² and this difference is crucial in the synthetic strategies followed by mussels in the process of adhesion.

There are extensive studies capitalizing on L-DOPA's redox chemistry with the goal of producing biomimetic adhesives for medical use and underwater adhesives in general,^{6,7} where technical adhesives are often lacking, particularly in environmental and biocompatibility.⁸

Besides their importance in natural adhesive processes, catechols play a key role in electric signaling in the human brain.⁹ L-DOPA is a neurotransmitter used in the treatment of Parkinson's disease and closely related to dopamine and adrenaline in its fundamental chemistry.¹⁰

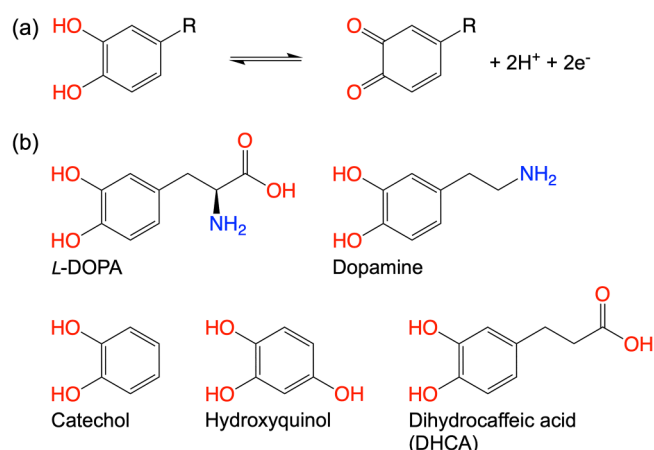


FIG. 1. (a) General oxidation mechanism of catechols. The attached group -R defines the functionalities and reactivity of the molecule. The particular substitutions and trivial names of the molecules used in this work are given in (b).

The electrochemical behavior of catechols is centered on the oxidation of the two hydroxyl groups, attached to the aromatic ring, to produce an *o*-quinone, as shown in Fig. 1. Other properties can be tuned by introducing changes to the side group -R. For instance, as an amino acid, L-DOPA contains both a -COOH and an -NH₂ group that give it an isoelectric point and make it prone to polymerize under certain conditions. The *pH* of the isoelectric point of L-DOPA is about 5.5–6. At this *pH* value, we will have a zwitterion in the solution, yet no auto-oxidation of the catechol.

Specifically in mussel foot proteins, L-DOPA can auto-oxidize, such as described by Yu *et al.*¹¹ High *pH* increases the likelihood of auto-oxidation and thus decreases the adhesion to surfaces such as mica.^{2,11} The importance of the interplay of oxidation and reduction in mussel byssus was further shown by Miller *et al.*¹² This suggests that the oxidation of L-DOPA must be carefully controlled, through its microenvironment, in order to keep constant, adhesive properties.¹³

For mussel foot attachment, the local *pH* has been probed using a *pH* indicator during initial injection of mfp by the mussels, and a strongly acidic *pH* of 2.5 was detected.¹⁴ This indicates the central role of the interplay of *pH* and L-DOPA redox chemistry during mussel foot attachment. Interestingly, it seems that the mussel closes off the local environment, generating a small volume that can effectively reach a much lower *pH* that is isolated from the neutral seawater.¹⁴

In contrast, commonly used surgical glues such as fibrin based tissue glues show decreased adhesive properties under wet saline conditions. Mussel foot adhesion has, therefore, been an inspiration for developing injectable¹⁵ and photo-activated¹⁶ biodegradable adhesives for wet tissue repair and as hemostatic agents.¹⁷

When developing new mussel inspired adhesives, this allows the use of *pH* to stabilize and manipulate the catechols' adhesive properties. To date, L-DOPA based bioadhesives are cross-linked through *pH* adjustment to nonacidic values.¹⁸ The disadvantage of such methods is the uncontrolled auto-oxidation of DOPA, which

inevitably accompanies a change in *pH*. In addition, changing the *pH* does not result in fast kinetics of polymer formation. However, the ability of the catechols to undergo redox processes makes them accessible to electrochemical analysis.^{19–22}

Furthermore, for medical procedures, the use of electrodes is state-of-the-art and electropolymerization may offer an interesting path into application of fast electrocuring catechol-based adhesives for biomedical applications. Here, we study the redox chemistry of L-DOPA and a range of molecules with the catechol functionality. We then use the information gained to design a bioadhesive that can be electrochemically cross-linked and surface grafted.

II. METHODS AND MATERIALS

A. Chemicals

L-DOPA (98 ± 1% purity) and dopamine hydrochloride (99% purity) were purchased from Alfa Aesar; sodium chloride (>99% purity) was purchased from Carl Roth; and all further chemicals were purchased from Sigma-Aldrich and are of the highest available grade (>98% purity). Poly(allylamine hydrochloride) (PAA), was obtained at a molecular weight of ~17 500). All solutions were prepared from Milli-Q water (Merck Millipore purification system, resistivity of 18.2 MΩ cm, TOC ≤ 2 ppb) at room temperature. Stock solutions of 100 mM NaClO₄ or 100 mM NaCl were prepared and *pH* adjusted to 5.5 by adding HCl or NaOH respectively.

B. Surface preparations

Homemade electrodes were produced by physical vapor deposition of 100 nm of gold onto a freshly cleaved mica sheet, at a pressure of ~2 × 10⁻⁶ Pa (system built at TU Wien). The gold side was glued to a 1 cm² glass slide using UV curable glue (NOA 81) from Norland Products Inc., and the mica was stripped off shortly before use allowing for a smooth, highly ordered gold surface.²³

C. Electrochemistry

All electrochemical experiments were performed at room temperature using a PalmSense4 potentiostat with a three electrode system. For experiments outside of quartz-crystal-microbalance measurements with dissipation analysis (QCM-D), gold template stripped from mica was used as the working electrode and a platinum mesh as the counter electrode. All potentials are referenced against an Ag/AgCl (3M KCl) reference electrode. Cleaning cycles were performed in argon bubbled NaCl or NaClO₄ before measurements. For single species cyclic voltammograms (CVs), 1 mM of the respective catechol was dissolved in 100 mM NaClO₄ *pH* 5.5 and kept under constant argon bubbling during measurements. CVs were performed at a scan rate of 100 mV/s after stabilization of the open circuit potential.

D. DHCA coupling to polymer

Catechol modified polyamine was synthesized as follows: (1) 0.63 g of DHCA was dissolved in 5.8 ml of 100 mM sodium chloride solution with an adjusted *pH* of 5.5. (2) 26.5 mg *N*-(3-dimethylaminopropyl)-*N*'-ethylcarbodiimide hydrochloride (EDC) and 80 mg of *N*-hydroxysuccinimide (NHS) were dissolved

in 2 ml of the same stock solution, and 0.2 ml was added to the DHCA solution. (3) 1.5 g of polyallylamine hydrochloride was dissolved in 6 ml of the same stock solution. (4) After 10 min, the two solutions were mixed and stored overnight in the dark. After 12 h, the solution appeared clear and light orange/brownish. (5) The pH of the solution was then slowly adjusted with swirling from $pH \approx 1.8$ to $pH = 5.5$ using 0.1 M NaOH. This solution was then degassed by Ar bubbling for at least 10 min before use in electropolymerization.

E. Electro-cross-linking of hydrogel

For electropolymerization, the electrodes were preconditioned in a NaCl solution by potential cycling (between -0.7 and 0.7 V vs Ag/AgCl) before being immersed in the pH adjusted and Ar bubbled polymer precursor solution. In experiments with template stripped Au electrodes, a potential of 0.4 V vs Ag/AgCl was applied for 60 s [Fig. 4(b)] or 20 s for surface forces apparatus (SFA) experiments and the current was measured using chronoamperometry.

F. Quartz-crystal-microbalance measurements with dissipation analysis

Gold coated quartz sensors were purchased from Biolin Scientific and used in a QSense E1 electrochemistry module. An Ag/AgCl (3M KCl) electrode was used as reference and a platinum sheet was used as a counter electrode. All solutions were degassed through constant argon bubbling before being pumped into the module at a flow rate of $50 \mu\text{l}/\text{min}$, at 24°C . After substantial flushing with Milli-Q water and performing cleaning cycles in 100 mM NaCl, the polymer solution was introduced and the electrodeposition was started. Chronopotentiometry was performed for 30 s and the potential was measured at a fixed current of 0.4 mA. During swelling of the hydrogel, the polymer solution flow was kept at a constant rate and switched back to the NaCl solution after equilibration of the layer thickness. Cyclic voltammograms were performed on the deposited film as seen in Fig. 4(c).

G. Surface forces apparatus measurements

Polymer films were prepared on template stripped 40 nm gold surfaces supported by curved cylindrical quartz surfaces with a curvature radius of 2 cm, using heat cured EPO-TEK-377 glue. The other cylinder, with a radius of curvature of 1 cm, supported a back-silvered mica sheet with 38 nm silver on UV cured Norland optical adhesive (NOA 81). Following a calibration measurement of a blank gold versus the mica sheet to determine the mica thickness (typically $4\text{--}8 \mu\text{m}$ thick), force measurements were performed on the polymer coated surfaces under three different conditions: hydrated in water (the surface was kept in water following deposition), dried (the surface was dried in air overnight before the measurements were taken also in air), and rehydrated (where the dried surface was resubmerged in water for 30 min and force measurements were taken in water). The force measurements were made with our SFA, which uses a load cell (strain gauges on a stiff spring) to sense the force independently from the distance measurement obtained from white light multiple beam interferometry.²⁴ The resultant fringes of equal chromatic order (FECO) are

projected into a spectrometer with a 2D sensor. The FECO images were analyzed for distance changes using the SFA explorer software also developed in house.²⁵ The refractive index used during the fitting for the polymer was a wavelength independent value of 1.478.

III. RESULTS AND DISCUSSION

Here, we first study the redox response of L-DOPA and related molecules shown in Fig. 1, and we aim to understand the electrochemical oxidation and potential subsequent degradation reactions of catechols. We then utilize the mechanistic understanding of catechol electrochemistry to synthesize and characterize a new bioadhesive and surface coating based on electrochemically triggered cross-linking.

Aiming to understand the electro-reactivity, Fig. 2 compares a set of cyclic voltammograms for different catechol molecules containing functional side groups (a)–(d), with the bare catechol (e) and hydroxyquinol (f), all dissolved in 100 mM NaClO₄ at pH 5.5. The bare catechol serves as a reference, which does not have the potential for any side reactions. Hydroxyquinol was added as a reference for potential side reactions that lead to the addition of an OH group to the benzene ring.

First, Figs. 2(a) and 2(b) show the redox response of amino acid- and amine-substituted catechols L-DOPA and dopamine, respectively. Both molecules show the same characteristic oxidation peak of the bare catechol control [Fig. 2(e)], with an oxidation potential around 0.32 V. The bare catechol shows a reversible redox behavior with no side reactions. Due to its structure, the only likely reactive part would be the oxidized hydroxyl groups on the benzene ring. If a quinone were to form a stable bond with the hydroxyl group of a reduced catechol or a water molecule, this would be visible in a change of the reduction peak height indicating a loss of material or a shift in the peak potential owing to a change on the ring. Therefore, we can rule out this type of interaction. However, both L-DOPA and dopamine show a decrease in current density over multiple scans, paired with the growth of a second oxidation peak at $0.5\text{--}0.6$ V, indicating a follow-up reaction at higher potentials.

This observation aligns well with a so-called ECE mechanism, which describes a consecutive set of reactions going from an initial electrochemical oxidation (E) of the catechol as shown in Fig. 1(a), followed by a chemical reaction (C), and a second electrochemical oxidation (E) as indicated by the peak at >0.5 V. This means, the presence of the amine and amino acid results in chemical follow-up reactions of the oxidized catechols with these functionalities. A dark precipitate of the degradation product, visible on the electrode after potential cycling, further confirms this.

As a potential chemical reaction, Brun and Rosset proposed, for example, hydroxyquinol formation as an intermediary step.¹⁹ To verify this, we can now compare the CVs of the substituted catechols to the redox behavior of hydroxyquinol [Fig. 2(f)]. The measured oxidation peak of hydroxyquinol at 0.15 V, however, does not overlap with any of the other measured peaks, rendering this intermediary highly unlikely.

The chemical step is even likely to vary between molecules. Figures 3(a) and 3(b) show possible reaction products of L-DOPA

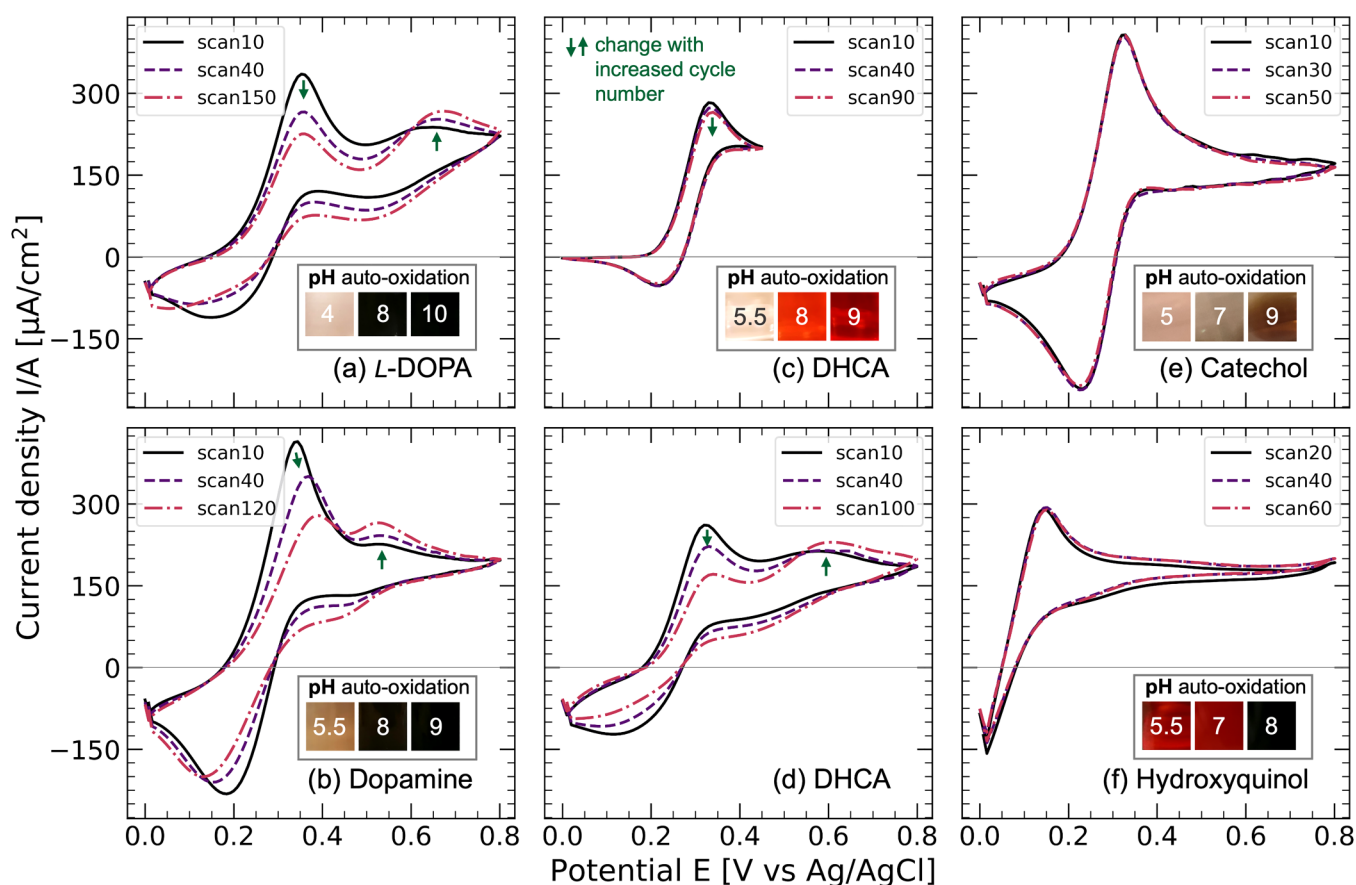


FIG. 2. CVs of respective catechols at 1 mM concentration in 100 mM NaClO₄ measured against Ag/AgCl. The arrows indicate the change of the peak position and intensity with increasing cycle number. For both (c) and (d), the solution is the same but the upper limit of the potential range was 0.45 V in (c) and 0.80 V in (d). Inlays show the color of the solutions at respective pH values after 2.5 h of auto-oxidation at 100 mM catechol concentrations.

and dopamine. During potential scanning, the oxidation peak position remains stable for L-DOPA [Fig. 2(a)] making chemical substitutions of the aromatic ring/ring-system unlikely. Instead, the nucleophilic amine attacks the oxidized catechol of a nearby L-DOPA molecule via a Schiff-base reaction, which can ultimately lead to the formation of extended polymeric chains. Hence, a chemically reacted catechol loses its electrochemical reaction ability, reducing the height of the peak, while the available catechols are unaltered in terms of their chemical environment (i.e., no shift of the oxidation peak).

In contrast, the oxidation peak of the dopamine shifts to higher potentials with increasing cycles, suggesting a change in the ring-system. This is consistent with a cyclization to an indole ring through a Michael addition before going further into the formation of melanin like aggregates. This mechanism among others was proposed by Schindler and Bechtold for pH > 8.²⁰

In summary, the chemical reaction step involves an intermolecular or intramolecular redox reaction without electron exchange with the electrode. Rather, it is a redistribution of redox states in

the chemical degradation product. Specifically, the formation of an L-DOPA dimer results in an oxidation of the carbon previously carrying an OH, while the nitrogen reduces [see oxidation states labeled in Fig. 3(a)]. Similarly, the formation of an aminochrome [Fig. 3(b)] from the dopamine results in an intramolecular charge reorganization, with the nitrogen-binding carbon increasing its oxidation state from -I to +I, while the carbons of the catechol functionality decrease their oxidation states from +II to +I. This Michael addition of the dopamine corresponds well with previous studies;²⁶ however, the dominance of Schiff-base reactions for L-DOPA is in contrast to studies indicating a lower change in Gibbs free energy for Michael additions than Schiff base reactions.²⁷ However, a Michael addition is clearly disproven by the missing shift in the first oxidation peak position in Fig. 2(a).

Second, we can now further compare electrochemical characteristics of a catechol that does not contain any amines/amino acids in the chemical structure. In particular, for DHCA, no quinone-amine reaction can take place, i.e., only the carboxylic acid can be active in potential chemical follow-up reactions with the oxidized

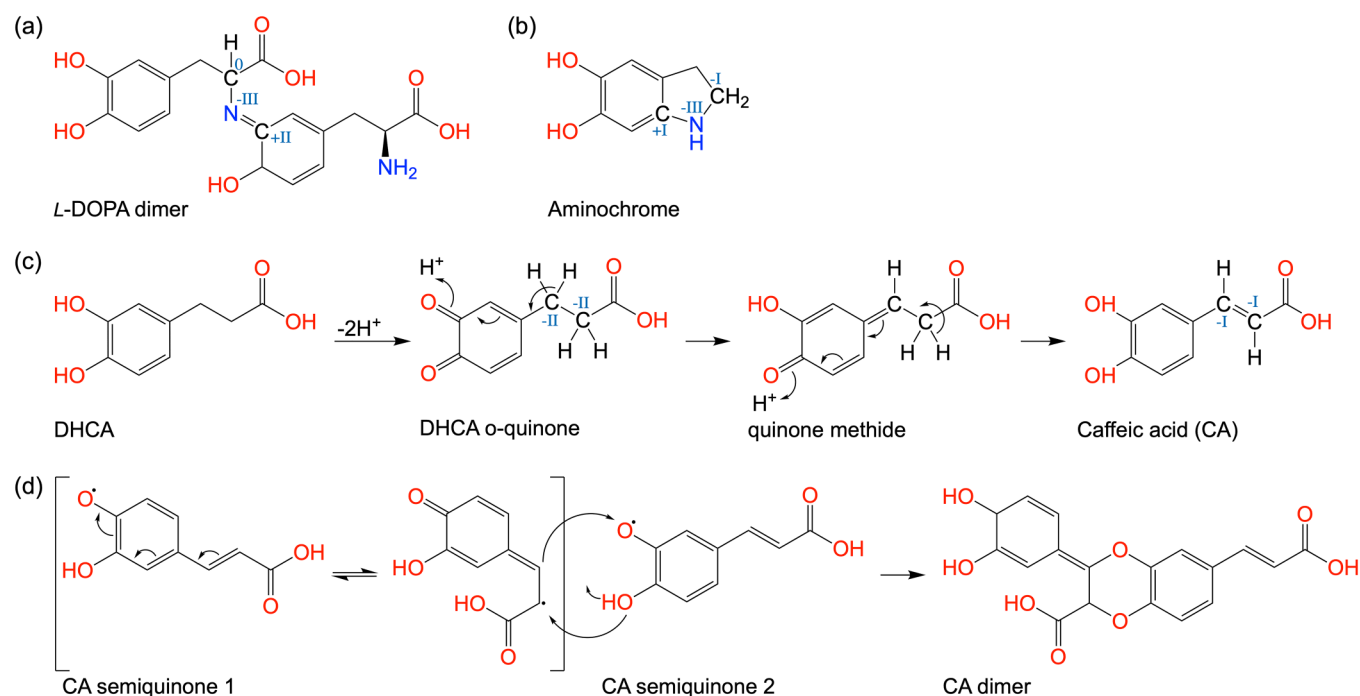


FIG. 3. Chemical degradation products after the initial oxidation and subsequent chemical reaction of the catechol for (a) L-DOPA: intermolecular Schiff-base reaction and (b) dopamine: intramolecular cyclization. DHCA: (c) degradation through a quinone methide intermediate to caffeic acid and (d) subsequent ionic Diels-Alder addition. Oxidation states for the key atoms are included in green.

form of the catechols. For DHCA, we show data for two different potential windows [Figs. 2(c) and 2(d)], which have a significant effect on subsequent CV cycles. When applying potentials below 0.45 V, the oxidation peak current density at 0.3 V remained relatively stable over the course of 90 scans. This indicates that this molecule does not immediately undergo a subsequent chemical reaction. In contrast, when running CVs in L-DOPA or dopamine, the decrease in the first oxidation peak current was independent of the potential scan range (see Fig. S1).²⁸

Coming back to DHCA [Fig. 2(d)], there was a strong decrease in the measured peak current over the same number of scans, in combination with an increasing second oxidation peak at 0.5 V, when higher potentials were applied. Again, the constant peak position of the first oxidation peak during scanning of a larger window again suggests a side chain reaction rather than a change in the aromatic ring structure. This precludes a cyclization of DHCA to dihydroresculetin as suggested previously.²⁹ The data instead support a tautomerization to quinone methide, in a slow process, followed by a more rapid auto-isomerization to caffeic acid esters.^{30,31} These structures have unsaturated side chains, which are stabilized by conjugation with the aromatic ring.

Figures 3(c) and 3(d) show a possible reaction pathway where, after a first oxidation process, quinone methide slowly degrades to caffeic acid (c), which after a second oxidation can dimerize (and ultimately polymerize) by an ionic Diels-Alder addition (d).

The described chemical reactivity of all compounds is further confirmed by visual inspection of pH adjusted catechol

solutions. The color box insets in Fig. 2 show the color of a 100 mM solution of the respective catechols after pH adjustment to the indicated pH values. Similar to electrochemistry, increase of pH equally shifts the equilibrium of oxidized and reduced forms toward the oxidized form. This can be inferred from the chemical reaction shown in Fig. 1(a), which will shift to the right-hand side if the proton concentration is lowered. Increase of the pH can hence initiate a process known as auto-oxidation and possible polymerization. The oxidized form can initiate a degradation based on chemical reactions seen in the redox characteristics.

All amine containing molecules, i.e., L-DOPA and dopamine, indicate the rapid formation of a black/dark precipitate due to an uncontrolled polymerization/degradation. This is effectively an equivalent to melanin routes observed e.g., during aging.³²

In contrast, molecules containing no amines indicate no precipitate formation, but still significant color changes, due to the change of the electron configurations in the polymerizing (but still soluble) aromatic systems (conjugation). For example, DHCA solution turns from an initial rose color into a dark reddish color. This is again consistent with a slower dimerization and no pronounced uncontrolled polymerization.

In summary, the higher stability and lower tendency for auto-oxidation compared to L-DOPA and dopamine make DHCA an attractive alternative for further use in catechol-based adhesive polymer and/or hydrogel design.

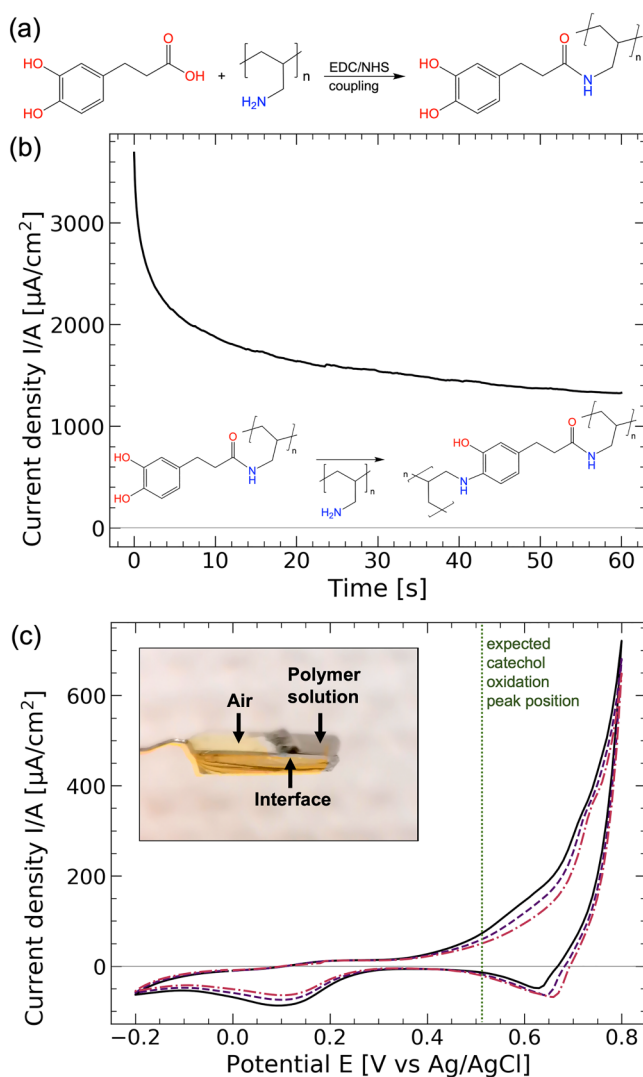


FIG. 4. (a) Schematic of DHCA coupling to PAA. (b) Electrochemical deposition and reaction scheme of polymer cross-linking at 0.4 V. (c) CV of a deposited hydrogel film in 100 mM NaCl on a gold surface (QCM-D crystal, see Sec. II for details). The dashed line shows the catechol oxidation potential. The absence of a peak at this position indicates that the polymer has fully cross-linked near the electrode interface. Inlay is an example of a deposited hydrogel film on a partially immersed electrode.

A. Catechol-based hydrogel

Catechol and amine cross-linking mechanisms have been used to develop multiple mussel inspired polymers as wet organic adhesives, which are of great interest for the development of tissue glues. Here, we aim to utilize DHCA as an alternative to dopamine and L-DOPA. It still offers the catechol functionality, while providing increased chemical/electrochemical stability. We aimed to synergistically combine both an amine functionality and the catechol

within the polymer³³ by chemically modifying a polyamine with DHCA that could be electrochemically cross-linked via a Schiff base reaction.

In detail, a DHCA modified poly(allylamine) (see Sec. II) was either cross-linked through alkaline pH adjustment to ≥ 8 or electropolymerized on a gold electrode. The ratio of amines on the PAA to DHCA molecules was 10:3, leaving enough free amines for cross-linking and adhesion promotion to a negatively charged substrate.

First, in the case of pH adjustment, a “skin” was formed at the air-liquid interface after about 24 h that continued to increase in thickness until the polymer aggregates in the solution were depleted. The rate of formation also depended on the pH, with higher pH values resulting in faster kinetics. When cut, this polymer layer showed self-healing properties within a few minutes, owing to the reservoir of polymer underneath the “skin” (see Fig. S2). This is in agreement with recently published results by Lee *et al.*³⁴ of a similar hydrogel that was cross-linked through pH adjustment and thoroughly tested. These properties may be enhanced further by introducing Fe^{3+} ions to make use of the catechol’s strong metal coordination capability³⁵ as has been shown previously.^{36,37}

When electrochemically cross-linking the polymer from the solution at pH 5.5, a hydrogel layer was formed by applying a constant potential. With increasing thickness of the layer the growth is slowed down as is visible in the current density decrease after several seconds of deposition [Fig. 4(b)]. Also, under electrochemical conditions, the growth at the air-water interface is visibly accelerated as seen in the inset in Fig. 4(c), where the growth was triggered at the air-water interface on purpose.

As further shown in Fig. 4(c), cyclic voltammograms of the deposited film, at 100 mV/s in 100 mM NaCl solution, showed that the majority of catechols close to the hydrogel-electrode interface were cross-linked through amine coupling to the PAA backbone and could no longer be oxidized (absence of oxidation peak at 0.32 V). Again, a standard three electrode setup was used, with an Ag/AgCl reference electrode and a gold coated QCM-D crystal as the working electrode. In addition, this might be interesting for future experiments, performing *in situ* electrochemical experiments on mussel feet during plaque formation through the electrochemical manipulation of the adherent surface.

B. Electrochemical deposition with QCM-D

For further analysis of the hydrogel film growth, QCM-D analysis was performed during chronopotentiometric deposition of the hydrogel combined with frequency and dissipation measurements. The modeling of the mass gain proved to be difficult as the large fluctuations in viscosity, shear force, and density disqualified Sauerbrey frequency modeling and constituted too many variables for conclusive Voigt-based viscoelastic modeling.

Hence, Fig. 5 only qualitatively shows the four determined phases of the electrodeposition. After the initial phase of constant NaCl solution flow at a rate of 50 $\mu\text{l}/\text{min}$, the switch to polymer solution in phase II leads to the absorption of noncross-linked polymer onto the gold surface. When the deposition current 0.4 mA is applied at the start of phase III, these aggregates start to

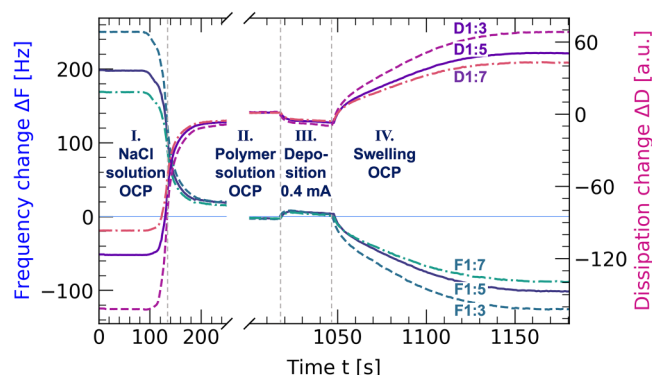


FIG. 5. QCM-D characterization of hydrogel deposition. Frequency and dissipation of overtones 3, 5, and 7 are displayed, labeled F1:3-7 and D1:3-7, respectively. Different phases are labeled I-IV (cf. text for details). The open circuit potential before deposition is typically at -0.1 to 0.0 V.

cross-link and the polymer is densely bound onto the electrode. In the following phase IV, the electrochemical deposition is stopped while the layer continues to grow substantially, as seen in the frequency changes, which we attribute to swelling, and it also undergoes large changes in viscosity and density as indicated by the dissipation change. When the hydrogel is well hydrated, the swelling stops and the layer stabilizes.

This layer had a strong adhesion to the gold electrode surface, which is evaluated in Sec. III C.

C. Hydrogel adhesion to mica

The adhesion was tested using two complementary experiments. First, we simply pressed a unit area normalized cleaned glass surface against an electrodeposited hydrogel film, and added load by hanging weights perpendicular (normal) to the surface on the formed contact. When two surfaces are coupled in such a way by this film, the system can sustain a load of ≥ 1.3 N/cm², with an adhesive failure at the glass/polymer interface. That is, we tested the adhesion of the outer surface of the formed polymer. Compared to the world record technical adhesive (3.4 kN/cm²),³⁸ this is a rather weak adhesion. However, for a wet system such as Tisseel, a fibrin based product (8.8 N/cm²)³⁹ used as a sealant in surgical applications, it is reasonably high and promises potential applications, in particular, considering that it can be swiftly cross-linked by applying an electrochemical potential. We also find that with some of these load tests, the adhesion failure occurred at the interface between the gold and the commercial UV glue, indicating that the adhesion at the electrochemically grown hydrogel-gold interface is even stronger than at the hydrogel-mica interface, at which the following measurements are taken.

We then further characterized the polymer hydrogel and quantified the adhesion in a SFA experiment. Specifically, the dried hydrogel samples were measured in air, whereas the wet and the rehydrated samples were measured in Milli-Q water. Figure 6(a) shows the measured approach of a negatively charged mica surface against the electrochemically grown hydrogel.

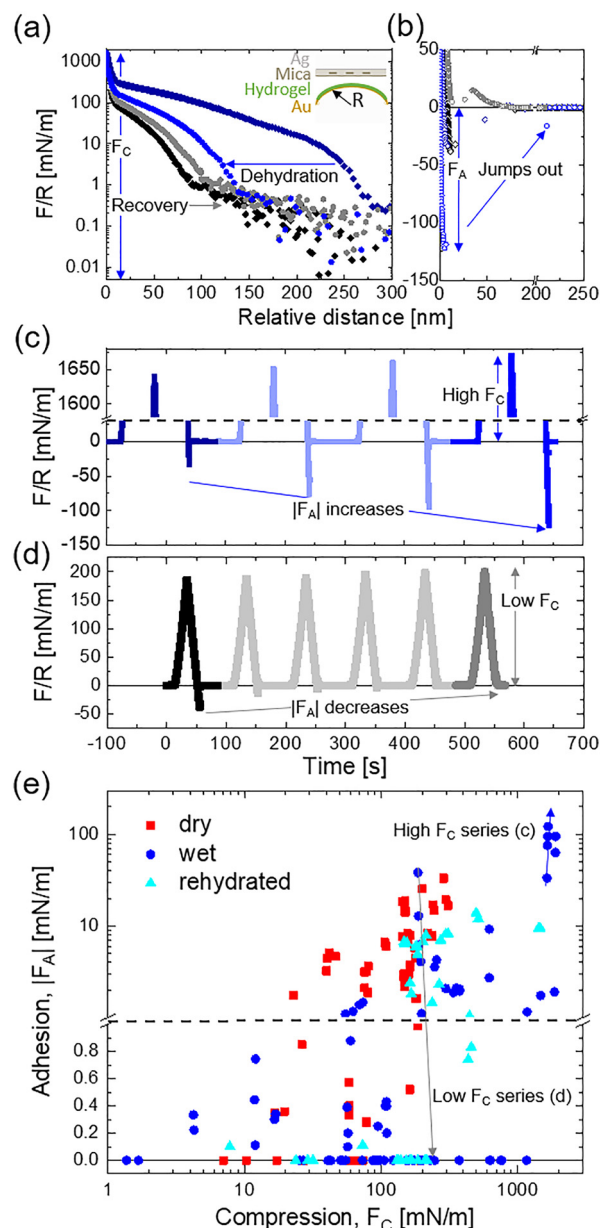


FIG. 6. SFA adhesion force measurements of hydrogel covered gold surfaces facing a mica surface [layers illustrated as inset in (a)] under various conditions. (a) Normalized force, F/R , vs distance characteristics during approach and (b) the adhesion minima, F_A , during the separation of the surfaces, for a wet hydrogel in water. The distance scale is relative to the minimum hard wall thickness recorded for the hydrogel film ~ 15 nm compared to the dry contact between the mica and the bare gold surface. In both (a) and (b), the dark and light blue points correspond to two cycles at high values of compression, F_C , and the black and gray points correspond to a lower F_C . These same force runs are illustrated against time in (c) for the high F_C values and in (d) for the lower ones. (e) Absolute adhesion force, $|F_A|$ map as a function of F_C under various sample and environmental conditions. Dry samples were measured in air and the rest in water.

First, the data show that the fully hydrated hydrogel is approximately 250 nm thick, based on the increase in force at around 250 nm, where the surface touches the hydrogel. Furthermore, the compression at increasing load indicates that the coating is highly compressible as expected for a hydrogel and can be dehydrated to 10% of its thickness at an applied load of 300 mN/m. During approach of the mica surface, the water is pushed out of the hydrogel layer leading to a roughly exponential increase in normalized force (F/R). Further compression leads to a change in the slope of the force-distance curve until a constant hard wall, where no further change in distance can be achieved. The plotted distance is relative to this fully compressed polymer thickness of approximately 15 nm. With repeated cycles at both high (dark to light blue) and low (black to gray) compression, although the overall thickness of the layer changes, the point at which the slope changes remains at around 11 nm from the minimum thickness (26 nm total thickness), suggesting that there is a change in the dehydration and hydrogel network rearrangement at this thickness. There is some recovery of the hydration when cycling continues at a lower compression (black to gray).

Next, in Fig. 6(b), the adhesion of the electrodeposited hydrogel film to the bare mica is shown during the separation of the surfaces. For high compressions (blue), the film is barely stretched at all before the mica jumps out of adhesion, whereas it recovers to 11–12 nm relative thickness before jumping out or back onto the repulsive curve for the low compression cycles (black/gray).

The adhesive minimum measured during separation strongly depends on the film properties (history and hydration state) and the amount of compression during approach. In Figs. 6(c) and 6(d), the effect of repeated cycling at high and low compressions, respectively, is highlighted in the force-time plots. At high compression, the gradual increase in adhesion is significant with only a minimal increase in the compression. With low compression, the adhesion decreases again but, although the adhesion indicates fewer catechol and amine bonds to the mica, the hydrated thickness does not recover easily during continued cycling even at a lower compression than that required for full dehydration.

Finally, Fig. 6(e) shows the measured adhesion as a function of applied load as well as hydration conditions. A higher compression was required in order to reach the hard wall for the wet samples that had never been dehydrated in air compared to the dry samples. The overall trend is that the maximum adhesion recorded increases with compression. On average, the dry samples show a higher adhesion in air than those measured in water, which is to be expected, due to the significantly reduced screening of interactions, such as van der Waals interactions, in air. Within each of the wet and rehydrated data sets, there are some further hydration effects caused by repeated cycling, as highlighted by the arrows associated with the high and low F_C series from panels (c) and (d).

Overall, the hydrogel showed adhesive strengths of ~ 4 mN/m and above at compressions of ~ 200 mN/m for wet samples, ~ 160 mN/m for rehydrated samples, and ~ 40 mN/m for dry samples in air. This threshold, of the upper adhesion values, is used as a comparison to the adhesion reported for mfp-5 by Lu *et al.* where the adhesion was not pressure dependent.³ For those instances where the adhesion remains below this value at higher F_C , the hydration, caused by the compression cycling history, is key to the final adhesion recorded. We can explain the adhesion increases by a

higher catechol and amine density at the dehydrated interface. There are three likely contributing factors. First, the hydrogel will have essentially collapsed in the dehydrated state increasing the density of the entire 3D network, implicitly increasing the catechol and amine density at the surface. Second, the reduced number of water molecules associated with the hydrogel network reduces the energy penalty associated with the bonds being formed between the amines/catechols and the mica. Finally, the increase in adhesion with repeated cycling seen in Fig. 6(c) could also be attributed to more adhesive groups becoming oriented to the outer surface of the hydrogel owing to slow rearrangement of the cross-linked polymer network, in addition to the dehydration effects.

With compression and dehydration, the hydrogel adhesive strength can, therefore, be significantly higher than that measured for mfp-3 and mfp-5 in aqueous solution at pH 5.5 with 1.4 and 4.6 mN/m, respectively, after 2 min of compression.³ Importantly, we note that the adhesion quantified here is of the outer surface of the hydrogel against the mica surface; the adhesion against the gold surface, at which it was electrochemically grown, is significantly stronger and never failed during the SFA experiments. In order to break the adhesion at the hydrogel-gold interface, both adhesion over the area and the cohesion of the hydrogel along the perimeter of the contact area would have to be smaller than the adhesion of the mica-hydrogel interface. Therefore, the cohesion of the hydrogel, close to the interface is also likely to be strong and contribute to there not being a failure of the gold-hydrogel interface even after multiple force runs. These are also both smooth surfaces and, therefore, the overall adhesion to a rough biomaterial could be higher from the increased effective surface area and opportunities for an interphase on a nanoscale.

IV. CONCLUSIONS

In this work, we studied the electrochemical characteristics of a comprehensive set of differently functionalized catechols. Specific conclusions can be summarized as follows:

- Based on the comprehensive set of molecules, electrochemical reaction mechanisms could be elucidated.
- Compared to nonfunctionalized catechols, all catechol molecules that contain amine, acid, or both functional groups indicate an ECE mechanism in CVs.
- The chemical steps indicated a consecutive intermolecular condensation as a Schiff-base reaction for L-DOPA, an ester formation of DHCA, or an intramolecular ring formation for dopamine after the first electrochemical oxidation of the catechol functionality.
- No hydroxyquinol formation was detected for the catechols used in this work.
- DHCA shows the least pronounced auto-oxidation tendency. It is also more stable and, hence, easier to control compared to L-DOPA. In particular, if the potential during oxidation is maintained below 0.45 V vs Ag/AgCl.
- This suggests that DHCA is a more stable and well controlled precursor for catechol-based polymer design for underwater adhesion.

- A novel polymeric hydrogel was electro-cross-linked based on DHCA modified polyamines, using the intermolecular Schiff-base reaction.
- In SFA measurements, the hydrogel showed high adhesion compared to previous work on mussel foot proteins at the outer water/polymer interface.
- On the electro-cross-linking substrate, the adhesion appeared considerably higher, that is, the polymer showed a strong attachment to the surface it grows on, combined with the cohesion of the hydrogel—in both dry and wet conditions.

Based on our findings, new and more stable as well as highly adhesive underwater glues may be developed. Our outlook is that further studies and simulations will help contextualize the reactivity of L-DOPA and L-DOPA modified peptides, with a great degree of control over the microenvironment. The strategy of combining catechols with other functional groups and amino acids in adhesives allow for synergy, in adhesion and reactivity, between different moieties to be explored. Also, subsequently developed polymers may form a reliable and reproducible electrochemically deposited coating for a range of applications, including corrosion inhibition and substrate modification for further chemical/structural modification for more complex interfacial architectures.²⁸

ACKNOWLEDGMENTS

The authors acknowledge the European Research Council for the support given through the ERC Grant No. 677663 (understanding of catechol electrochemistry) and the Austrian Research Promotion Agency FFG in the framework of the COMET Center of Electrochemistry and Surface Technology, CEST, through Grant No. 865864 (biomaterial synthesis, biomimetic glues, and coatings). The authors also acknowledge the TU Wien University Library for financial support through its Open Access Funding Program.

DATA AVAILABILITY

The raw and processed data required to reproduce these findings are available from the corresponding authors via www.repositum.tuwien.ac.at upon reasonable request.

REFERENCES

¹J. Waite, *Int. J. Adhes. Adhes.* **7**, 9 (1987).
²H. Lee, N. Scherer, and P. Messersmith, *Proc. Natl. Acad. Sci. U.S.A.* **103**, 12999 (2006).
³Q. Lu, E. Danner, J. Waite, J. Israelachvili, H. Zeng, and D. Hwang, *J. R. Soc. Interface* **10**, 20120759 (2013).
⁴J. Yu, W. Wei, E. Danner, R. K. Ashley, J. N. Israelachvili, and J. H. Waite, *Nat. Chem. Biol.* **7**, 588 (2011).
⁵H. Silverman and F. Roberto, *Mar. Biotechnol.* **9**, 661 (2007).
⁶J. Suppan, B. Engel, M. Marchetti-Deschmann, and S. Nürnbergger, *Biol. Rev.* **93**, 1056 (2018).

⁷T. Reece, T. Maxey, and I. Kron, *Am. J. Surg.* **182**, S40 (2001).
⁸P. Leggat, D. Smith, and U. Kedjarune, *ANZ J. Surg.* **77**, 209 (2007).
⁹A. Bjorklund and S. Dunnett, *Trends Neurosci.* **30**, 194 (2007).
¹⁰S. Chen and K. Peng, *J. Electroanal. Chem.* **547**, 179 (2003).
¹¹J. Yu, W. Wei, E. Danner, J. Israelachvili, and J. Waite, *Adv. Mater.* **23**, 2362 (2011).
¹²D. R. Miller, J. E. Spahn, and J. H. Waite, *J. R. Soc. Interface* **12**, 20150614 (2015).
¹³W. Wei, J. Yu, C. Broomell, J. Israelachvili, and J. Waite, *J. Am. Chem. Soc.* **135**, 377 (2012).
¹⁴N. Martinez Rodriguez, S. Das, Y. Kaufman, J. N. Israelachvili, and J. Waite, *Biofouling* **31**, 221 (2015).
¹⁵M. Mehdizadeh, H. Weng, D. Gyawali, L. Tang, and J. Yang, *Biomaterials* **33**, 7972 (2012).
¹⁶E. Y. Jeon, B. H. Hwang, Y. J. Yang, B. J. Kim, B.-H. Choi, G. Y. Jung, and H. J. Cha, *Biomaterials* **67**, 11 (2015).
¹⁷P. T. M. Phuong, H. J. Won, Y. J. Oh, H. S. Lee, K. D. Lee, and S. Y. Park, *J. Ind. Eng. Chem.* **80**, 749 (2019).
¹⁸B. P. Lee, P. Messersmith, J. Israelachvili, and J. Waite, *Annu. Rev. Mater. Res.* **41**, 99 (2011).
¹⁹A. Brun and R. Rosset, *J. Electroanal. Chem. Interfacial Electrochem.* **49**, 287 (1974).
²⁰S. Schindler and T. Bechtold, *J. Electroanal. Chem.* **836**, 94 (2019).
²¹M. Eslami, M. Namazian, and H. Zare, *Electrochim. Acta* **88**, 543 (2013).
²²M. Eslami, H. Zare, and M. Namazian, *J. Phys. Chem. B* **116**, 12552 (2012).
²³L. Chai and J. Klein, *Langmuir* **23**, 7777 (2007).
²⁴V. Wieser, P. Bilotto, U. Ramach, H. Yuan, K. Schwenzfeier, H.-W. Cheng, and M. Valtiner, *J. Vac. Sci. Technol. A* **39**, 023201 (2021).
²⁵K. A. Schwenzfeier, A. Erbe, P. Bilotto, M. Lengauer, C. Merola, H.-W. Cheng, L. L. Mears, and M. Valtiner, *Rev. Sci. Instrum.* **90**, 043908 (2019).
²⁶W.-Z. Qiu, G.-P. Wu, and Z.-K. Xu, *ACS Appl. Mater. Interfaces* **10**, 5902 (2018).
²⁷J. Yang, V. Saggiomo, A. H. Velders, M. A. Cohen Stuart, and M. Kamperman, *PLoS ONE* **11**, e0166490 (2016).
²⁸See the supplementary material at <https://www.scitation.org/doi/suppl/10.1116/6.0001609> for additional cyclic voltammograms of L-DOPA and dopamine, self-healing images.
²⁹M. Sugumaran, H. Dali, H. Kundzicz, and V. Semensi, *Bioorg. Chem.* **17**, 443 (1989).
³⁰S. Ito, M. Sugumaran, and K. Wakamatsu, *Int. J. Mol. Sci.* **21**, 6080 (2020).
³¹M. Sugumaran, *Int. J. Mol. Sci.* **17**, 1576 (2016).
³²A. Skoczyńska, E. Budzisz, E. Trznadel-Grodzka, and H. Rotsztein, *Adv. Dermat. Allergol.* **34**, 97 (2017).
³³M. V. Rapp, G. P. Maier, H. A. Dobbs, N. J. Higdon, J. H. Waite, A. Butler, and J. N. Israelachvili, *J. Am. Chem. Soc.* **138**, 9013 (2016).
³⁴J. N. Lee, S. Y. Lee, and W. H. Park, *ACS Appl. Mater. Interfaces* **13**, 18324 (2021).
³⁵H. Zeng, D. S. Hwang, J. N. Israelachvili, and J. H. Waite, *Proc. Natl. Acad. Sci. U.S.A.* **107**, 12850 (2010).
³⁶M. Krogsgaard, M. A. Behrens, J. S. Pedersen, and H. Birkedal, *Biomacromolecules* **14**, 297 (2013).
³⁷Z. Jia, Y. Zeng, P. Tang, D. Gan, W. Xing, Y. Hou, K. Wang, C. Xie, and X. Lu, *Chem. Mater.* **31**, 5625 (2019).
³⁸See <https://www.guinnessworldrecords.com/world-records/heaviest-weight-lifted-with-glue> for Guinness World Records, 2019.
³⁹D. G. Wallace, *et al.*, *J. Biomed. Mater. Res.* **58**, 545 (2001).